VSP

Journal of Biomaterials Science 22 (2011) 1069–1082

Journal of BIOMATERIALS SCIENCE
brill.nl/jbs

Electrospun Silk Fibroin–Hydroxybutyl Chitosan Nanofibrous Scaffolds to Biomimic Extracellular Matrix

Kuihua Zhang [a,b,c], **Yongfang Qian** [b], **Hongsheng Wang** [b], **Linpeng Fan** [b], **Chen Huang** [b] **and Xiumei Mo** [a,b,*]

[a] State Key Laboratory for Modification of Chemical Fibres and Polymer Materials, College of Materials Science and Engineering, Donghua University, Shanghai 201620, P. R. China
[b] Biomaterials and Tissue Engineering Lab, College of Chemistry and Chemical Engineering and Biological Engineering, Donghua University, 2999 Renmin Road North, Songjiang District, Shanghai 201620, P. R. China
[c] College of Biological Engineering and Chemical Engineering, Jiaxing College, Zhejiang 314001, P. R. China

Received 3 December 2009; accepted 17 March 2010

Abstract

Silk fibroin (SF)–hydroxybutyl chitosan (HBC) blend nanofibrous scaffolds were fabricated using 1,1,1,3,3,3-hexafluoro-2-propanol (HFIP) and trifluoroacetic acid (TFA) as solvents to biomimic the native ECM by electrospinning. SEM results showed that the average nanofibrous diameter increased when the content of HBC was raised from 20% to 100%. Whereas water contact angle measurements confirmed that SF/HBC nanofibrous scaffolds with different weight ratios were of good hydrophilicity. Both the tensile strength and the elongation at break were improved obviously when the weight ratio of SF to HBC was 20:80. ^{13}C-NMR clarified that SF and HBC molecules existed in H-bond interactions, but HBC did not induce SF conformation to transform from random coil form to β-sheet structure. Moreover, the use of genipin vapour not only induced conformation of SF to convert from random coil to β-sheet structure but also acted as a cross-linking agent for SF and HBC. Cell viability studies demonstrated that SF/HBC nanofibrous scaffolds presented good cellular compatibility. Thus, electrospun SF/HBC blended nanofibres may provide an ideal biomimic tissue-engineering scaffold.

Keywords

Electrospinning, silk fibroin–hydroxybutyl chitosan, scaffold, tissue engineering

* To whom correspondence should be addressed. Tel.: (86-21) 6779-2653; Fax: (86-21) 6779-2653; e-mail: med@dhu.edu.cn

DOI:10.1163/092050610X498204

1. Introduction

In living systems, the extracellular matrix (ECM) plays a pivotal role in controlling cell behaviour [1]. It provides resident cells with specific ligands for cell attachment and migration, and modulates cell proliferation and function [2–4]. Therefore, the ideal tissue-engineering scaffold should mimic the chemical composition, physical structure and biological function of native extracellular matrix (ECM) as much as possible [5]. The native ECM is composed of a cross-linked porous network of multifibril collagens with diameters ranging from 50 to 500 nm and embedded in glycosaminoglycans [1, 6, 7].

Silk fibroin (SF) is an attractive natural fibrous protein for biomedical applications due to its unique properties, including good biocompatibility, biodegradability, lower inflammatory response than collagen and commercial availability at relatively low cost [8, 9]. Chitosan, a kind of natural polysaccharide, has also been widely applied in pharmaceutical and medical fields due to good biocompatibility, biodegradability, antibacterial activity and various biofunctionalities, including antithrombogenic, hemostaticimmunity enhancing and wound-healing properties [10]. Hydroxybutyl chitosan (HBC) is fabricated by conjugation of hydroxybutyl (HB) groups to the hydroxyl and amino-reactive sites of chitosan. This modification could increase the solubility of chitosan in water or organic solution and electrospinability [11], while still maintaining the excellent properties of chitosan [12, 13]. Generally prepared as casting films, porous sponges and patches, recently silk fibroin and chitosan blends have been widely studied as biomaterials in tissue-engineering fields to further biomimic components of the native ECM [14, 15]. Meanwhile, biomimic non-woven scaffolds generated by electrospinning have been composed of a large network of interconnected fibres and pores, resembling the topographic features of the ECM [16]. Therefore, electrospun SF/HBC blend nanofibrous scaffolds may develop a novel kind of scaffolds to biomimic the structure and component of ECM for tissue engineering or functional biomaterials.

Park *et al*. [17] reported the electrospinning of silk fibroin (SF)/chitosan (CS) blends with formic acid as a spinning solvent, but the properties and cytocompatibility were not studied. In the present study, SF/HBC blend nanofibres at different weight ratios were fabricated with blends of 1,1,1,3,3,3-hexafluoro-2-propanol (HFIP) and trifluoroacetic acid (TFA) (volume ratio 90:10) as solvents. The morphology, structure and properties of the SF/HBC nanofibre scaffolds were investigated by SEM, ^{13}C-NMR, water contact angle and tensile measurement. To assess the cytocompatibility of SF/HBC nanofibrous scaffolds, pig iliac endothelial cells (PIECs) were used to study the cell interaction with blend nanofibrous scaffolds.

2. Materials and Methods

2.1. Materials

Cocoons of *Bombyx mori* silkworm were kindly supplied by Jiaxing Silk. Hydroxybutyl chitosan (HBC, 85%, deacetylated) was kindly provided by Shanghai

Qisheng Biological Agents. 1,1,1,3,3,3-Hexafluoroisopropanol (HFIP) from Fluorochem and trifluoroacetic acid (TFA) from Sinopharm Chemical Reagent were used as solvents.

2.2. Preparation of Regenerated SF

Raw silk was degummed three times with 0.5% (w/w) Na_2CO_3 solution at 100°C for 30 min each and then washed with distilled water. Degummed silk was dissolved in a ternary solvent system of $CaCl_2/H_2O$/EtOH solution (1:8:2 mol ratio) for 1 h at 70°C. After dialysis with a cellulose tubular membrane (250-7u; Sigma) in distilled water for 3 days at room temperature, the SF solution was filtered and lyophilized to obtain the regenerated SF sponges.

2.3. Electrospinning

SF was dissolved in HFIP and HBC was dissolved in HFIP/TFA (90:10, v/v) at various concentrations, respectively. When they were prepared already, the two solutions were blended at different weight ratios with sufficient stirring at room temperature before electrospinning. The solutions were placed into a 2.5 ml plastic syringe with a blunt-ended needle with an inner diameter of 0.21 mm. The needle was located at a distance of 15 mm from the grounded collector. A syringe pump (Cole-Parmer 789100C) was used to feed solutions to the needle tip at a feed rate of 0.5–1.0 ml/h. A high electrospinning voltage was applied between the needle and ground collector using a high voltage power supply (BGG6-358, BMEICO). The applied voltage was 20 kV.

2.4. Characterization

The morphology and diameter of the electrospun fibres was observed with a scanning electronic microscope (SEM; JSM-5600) at an accelerating voltage of 10 kV. The diameter range of the fabricated ultrafine fibres was measured based on the SEM images using image J 1.34s (NIH) image visualization software and calculated by selecting 100 fibres randomly observed on the SEM images.

The ^{13}C-CP–MAS-NMR spectra of the electrospun scaffolds were obtained using a NMR spectrometer (Bruker AV400) with a ^{13}C resonance frequency of 100 MHz, contact time of 1.0 ms, pulse delay time of 4.0 s.

2.5. Contact Angle Measurements

Surface wettabilities of the electrospun scaffolds were characterized by water contact angle measurement. Distilled water (0.03 ml) was carefully dropped onto the electrospun scaffolds. The images of the droplet on the scaffolds were visualized through the image analyzer (Datephysics OCA40) and the angles between the water droplet and the surface were also measured. To confirm the uniform distribution of blend nanofibrous scaffolds, every sample was measured 3 times from different positions and an average value was calculated using a statistical method.

2.6. Pore Size Measurements

An CFP-1100-AI capillary flow porometer (PMI Porous Materials) was used in this study to measure the pore size. Calwick (PMI Porous Materials), with a defined surface tension of 21 dyne/cm, was used as the wetting agent for porometry measurements. Electrospun nanofibrous scaffolds were cut into 3 cm × 3 cm squares for porometry measurement.

2.7. Mechanical Measurement

The mechanical properties were obtained by applying tensile test loads to specimens prepared from the electrospun scaffolds with different SF/HBC blend weight ratios (100:0, 80:20, 50:50, 20:80, 0:100). In this study, specimens were prepared according to the method described by Huang *et al*. [18]. First, a white paper was cut into a template with width × gauge length, and double-side tapes were glued onto the top and bottom areas of one side. The template was then glued onto top side of the fibre scaffold, and was cut into rectangular pieces along the vertical lines. After the aluminium foil was carefully peeled off, single-sided tapes were applied onto the gripping areas as end-tabs. The resulting specimens had a planar dimension of width × gauge length = 10 mm × 30 mm. The mechanical properties were tested by a materials testing machine (Hounsfield H5K-S) at a temperature of 20°C, a relative humidity of 65% and a elongation speed of 10 mm/min. Wet state samples were also measured after soaking cross-linked electrospun scaffolds in deionized water for 1 h and the water on the surface of scaffolds was blotted with filter paper. The specimen thicknesses were measured using a digital micrometer, having a precision of 0.01 mm.

2.8. Cross-linking

Genipin was dissolved in ethanol at a concentration of 50 mg/ml, and the solution was put into a desiccator. SF/HBC nanofibrous scaffolds were fixed in the desiccator saturated with genipin vapour at 25°C for 24 h and then dried in a vacuum at room temperature for 24 h.

2.9. Viability of PIECs on Nanofibrous Scaffolds

Pig iliac endothelial cells (PIECs) were cultured in DMEM medium with 10% foetal bovine serum and 1% antibiotic–antimycotic in an atmosphere of 5% CO_2 and 37°C, and the medium was replenished every 3 days. Electrospun scaffolds were prepared on circular glass coverslips (14 mm in diameter) and the coverslips were fixed in 24-well plates with a stainless ring. Before seeding cells, scaffolds were sterilized by immersion in 75% ethanol for 2 h, washed 3 times with phosphate-buffered saline solution (PBS), and then washed once with the culture medium.

Cell viability on electrospun scaffolds, coverslips and tissue-culture plates (TCP) was determined using the MTT method. Briefly, the cell and matrices were incubated with 3-[4,5-dimehyl-2-thiazolyl]-2,5-diphenyl-2H-tetrazolium bromide

(MTT, 5 mg/ml) for 4 h. Thereafter, the culture media were extracted and 400 µl dimethylsulfoxide (DMSO) was added or about 20 min. When the crystal was sufficiently resolved, aliquots were pipetted into the wells of a 96-well plate and tested by an enzyme-labeled instrument (Thermo MK3), and the absorbance at 570 nm was measured for each well.

For the proliferation study, endothelial cells were seeded onto fibre scaffolds, glass coverslips and TCP ($n = 4$) at a density of 1.0×10^4 cells/well for 1, 3, 5 and 7 days. After cell seeding, unattached cells were washed out with PBS solution and attached cells were quantified by MTT method.

After 3 days of culturing, the electrospun fibrous scaffolds with cells (density 1.0×10^4 cells/well) were examined by SEM. the scaffolds were rinsed twice with PBS and fixed in 4% glutaraldehyde water solution at 4°C for 2 h. Fixed samples were rinsed twice with PBS and then dehydrated in graded concentrations of ethanol (30, 50, 70, 80, 90, 95 and 100%). Finally, they were dried in vacuum overnight. The dry cellular constructs were sputter-coated with gold and observed under the SEM at a voltage of 10 kV.

2.10. Statistical Analysis

Statistical analysis was performed using Origin 7.5 (Origin Lab). Values (at least triplicate) were averaged and expressed as means ± SD. Statistical differences were determined by one-way ANOVA and differences were considered statistically significant at $P < 0.05$.

3. Results and Discussion

3.1. Morphology of SF/HBC Blend Nanofibres

In the electrospinning process, we found that SF could be dissolved in HFIP and become electrospinnable, but a gel was formed and no fibre could be spun due to the high viscosity when HBC was dissolved in HFIP. Hence, TFA was added into the solution of HBC in HFIP to improve the HBC solution because TFA forms salts with the amino groups of HBC and this salt formation destroys the rigid interaction between the chitosan molecules, making them ready to be electrospun [19]. A mixture of HFIP and TFA (90:10, v/v) was selected as an appropriate solvent for electrospinning of HBC. Through adjusting the SF and HBC concentration, we selected 12% (w/v) SF and 6% (w/v) HBC as the working concentration for different ratios of SF/HBC mixture. The electrospun nanofibres with different blend ratios of SF/HBC from 100:0 to 0:100 were fabricated. The SEM micrographs and average diameters of electrospun blend nanofibres are shown in Fig. 1. The average diameter of pure SF nanofibres was 215 ± 84.0 nm. The fibre average diameter increased to 313 ± 151.1 nm after adding 20% HBC, because of the increasing viscosity of blend solutions, whereas fibre average diameters gradually deceased from 313 ± 151.1 nm to 107 ± 77.4 nm with further increasing HBC content in the blend. This phenomenon could be explained by the conductivity increase of the blend solution with

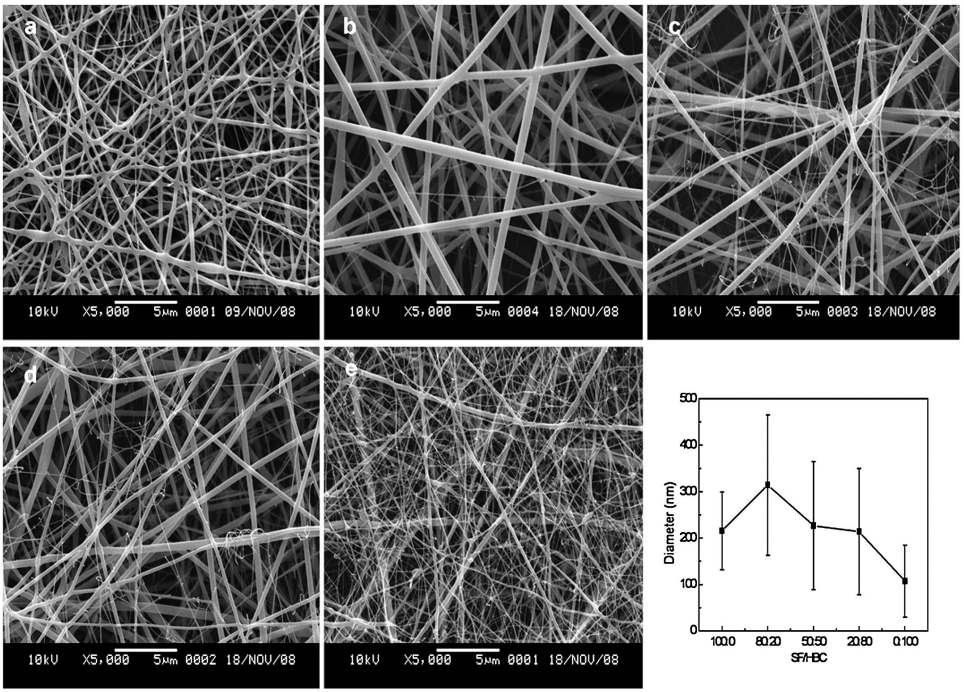

Figure 1. SEM images and average diameters at 2% (w/v) SF/6% (w/v) HBC with different weight ratios: (a) 100:0, (b) 80:20, (c) 50:50, (d) 20:80 and (e) 0:100.

increasing HBC content. Since chitosan is a typical cationic polyelectrolyte, more ions were formed in the blend solution when HBC content increased, thus, increase the solution conductivity. On the other hand, the increased charge density will lead to larger elongation forces for the fibre jet to yield smaller fibres [20].

3.2. Structure of the SF/HBC Blend Nanofibres

Solid-state ^{13}C-NMR has been shown to be a more effective structure analytical tool for polymers. The secondary structure of *Bombyx mori* SF consists of the major conformations, including random coils or helix (silk I) and β-sheet (silk II) [21]. The β-sheet form can be identified by the ^{13}C chemical shifts of Gly (glycine), Ser (serine) and Ala (alanine) that are indicative of β-sheet conformations. Particularly, the chemical shift of alanyl C$^{\beta}$ is an excellent indicator for the silk fibroin conformation. Zhou *et al*. [22] illustrated that the chemical shifts in Ala residues of C$^{\beta}$ within 18.5–20.5 ppm were assigned to β-sheet conformation (silk II) and the chemical shifts in Ala residues of C$^{\beta}$ within 14.5–17.5 ppm could be assigned to random coils or helix (silk I). The higher chemical shifts in Ala residues of C$^{\beta}$ indicated a higher β-sheet conformation content [23]. The ^{13}C-NMR spectra of pure SF, HBC and SF/HBC blended nanofibrous scaffolds are shown in Fig. 2. In the ^{13}C-NMR spectra of HBC nanofibrous scaffolds, the peaks at 97.88, 56.64, 71.41, 82.45, 74.88 and 26.80 ppm were attributed to C1, C2/C6, C3, C4, C5 and

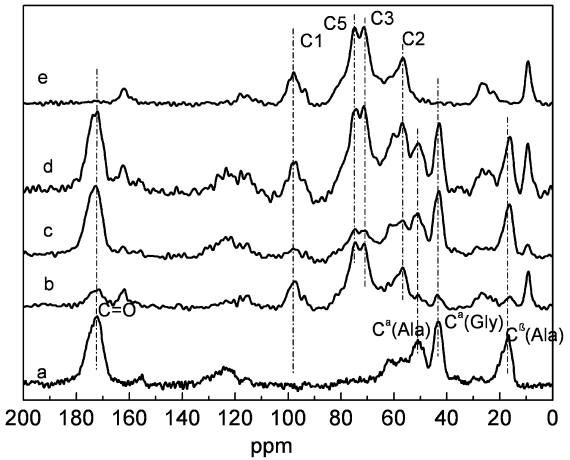

Figure 2. ^{13}C-CP/MAS-NMR spectra of SF/HBC blend nanofibres: (a) 100:0, (b) 80:20, (c) 50:50, (d) 20:80 and (e) 0:100.

methylene/methyl of HBC [24]. In the ^{13}C-NMR spectra of pure SF nanofibrous scaffolds, the peaks at 172.2, 60.6, 50.9, 43.3 ppm were attributed to carbonyl carbons of SF, C^{β} of Ser, C^{α} of Ala and C^{α} of Gly [25]. The ^{13}C-NMR spectra of SF/HBC blend nanofibrous scaffolds showed the characteristic chemical shifts of both SF and HBC. However, after blending with different ratios, the intensity of some characteristic peaks changed; the peak intensities of the carbonyl carbons, C^{β} of Ala of SF, decreased obviously when blended with 80:20, peak intensities of C1, C2, C3, C5 and methylene/methyl of HBC decreased when blended with 50:50. These peak intensities were not proportional to the content of SF or HBC. Meanwhile, we found chemical shifts of them showed slight changes. The results demonstrated that SF and HBC molecules presented H-bond interactions, which led to the change of carbon chemical microenvironment. The chemical shifts of C^{β} of Ala showed HBC did not induce conformation of SF to transform from random coil to β-sheet structure.

The ^{13}C-NMR spectra for electrospun and blend nanofibres (20:80) cross-linked with genipin vapour and their expanded ^{13}C-CP/MAS-NMR spectra of the methyl regions of Ala are shown in Figs 3 and 4. The chemical shift of Ala C^{β} in SF nanofibres varied from 16.2 ppm for random coils or helix to 20.7 ppm for β-sheet conformation after cross-linking with genipin vapour. Meanwhile, the chemical shift of carbonyl carbons of SF transformed from 172.0 ppm to 173.3 ppm with an obvious decrease of peak intensity. The chemical shift of C2 bond NH_2 in HBC and C^{α} bond NH_2 of Gla in SF transformed from 57.1 ppm to 56.1 ppm and from 42.9 ppm to 43.5 ppm, respectively, which could be explained by the reaction of amino groups of SF and HBC with genipin. The results demonstrated that genipin vapour not only induced SF conformation to convert from random coil to β-sheet but also acted as a cross-linking agent for SF and HBC.

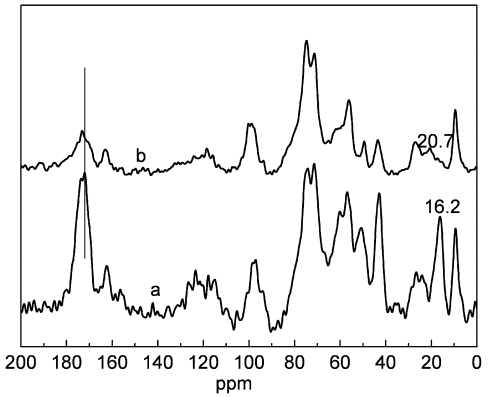

Figure 3. ^{13}C-CP/MAS-NMR spectra of SF/HBC (20:80) blend nanofibres before and after cross-linking: (a) non-cross-linked and (b) cross-linked.

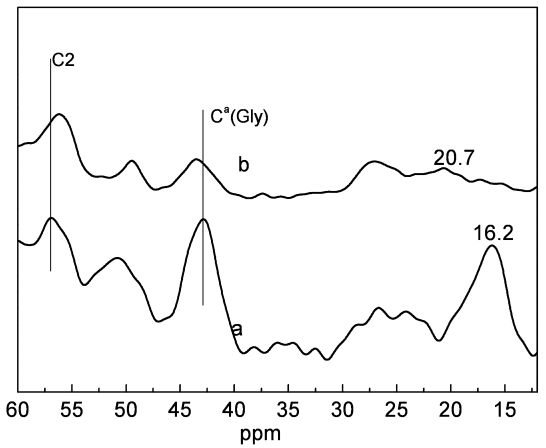

Figure 4. Expanded ^{13}C-CP/MAS-NMR spectra of SF/HBC (20:80) blend nanofibres before and after cross-linking: (a) non-cross-linked and (b) cross-linked.

3.3. Water Contact Angle Analysis

The surface wettability plays an important role in affecting cell attachment, proliferation and migration [26–28]. To clarify surface properties of electrospun SF/HBC nanofibrous scaffolds, water contact angles of nanofibrous scaffolds before and after cross-linking with genipin vapour were measured and shown in Fig. 5. The results showed that pure SF nanofibrous scaffolds were ultra-hydrophilic because of its hydrophilic groups and random coil conformation. With the increasing HBC content, water contact angle on nanofibrous scaffolds gradually increased. The results showed hydrophilicity gradually decreased along with the increase of HBC content. Generally, water contact angles of SF/HBC nanofibrous scaffolds with different ratios were less than 90°. Compared with non-cross-linked nanofibrous scaffolds, all the water contact angles increased to some extent after the nanofibrous scaffolds

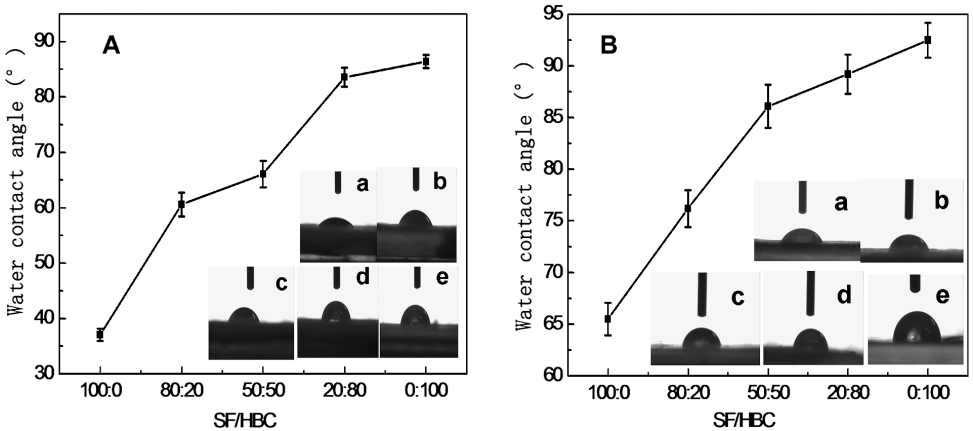

Figure 5. Water contact angles of SF/HBC blend nanofibrous scaffolds (A) before and (B) after cross-linking: (a) 100:0, (b) 80:20, (c) 50:50, (d) 20:80 and (e) 0:100.

Table 1.
Pore diameter of SF/HBC nanofibrous scaffolds with various blend ratios

SF/HBC weight ratio	Specimen thickness (mm)	Mean flow pore diameter ± SD (μm)	Largest pore diameter (μm)	Smallest pore diameter (μm)
100:0	0.068	0.8174 ± 0.3110	1.8451	0.5592
80:20	0.130	0.5422 ± 0.2866	1.7518	0.3284
50:50	0.114	0.5653 ± 0.2459	1.6020	0.3035
20:80	0.036	0.4407 ± 0.1777	1.1664	0.2362
0:100	0.023	0.2490 ± 0.0397	0.4300	0.2074

were cross-linked, attributed to the transformation of SF conformation from random coil to β-sheet and the physical entanglements formed among nanofibres.

3.4. Pore Diameter and Mechanical Properties Analyses

Electrospun nanofibrous scaffolds with micro-scale and nanoscale porous structure are most favourable for tissue-engineering scaffolds because the highly porous network of interconnected pores provides nutrients and gas exchange, which are crucial for cellular growth and tissue regeneration [29]. Pore diameters of SF/HBC nanofibrous scaffolds with various blend ratios are shown in Table 1. Mean flow pore diameter of pure SF was 0.8174 ± 0.3110 μm. When the blend weight ratio of SF and HBC was 80:20, the mean flow pore diameter was 0.5422 ± 0.2866 μm. This value gradually decreased when blend weight ratios of SF and HBC varied from 50:50 to 0:100. It was reported that pore size is strongly associated with fiber mass, fibre thickness, fibre diameter and fibre length. An increase in fibre mass and thickness caused a decrease in pore size. Fibre diameter plays a dominant role in controlling pore diameter of scaffolds, decreasing fibre diameter results in a de-

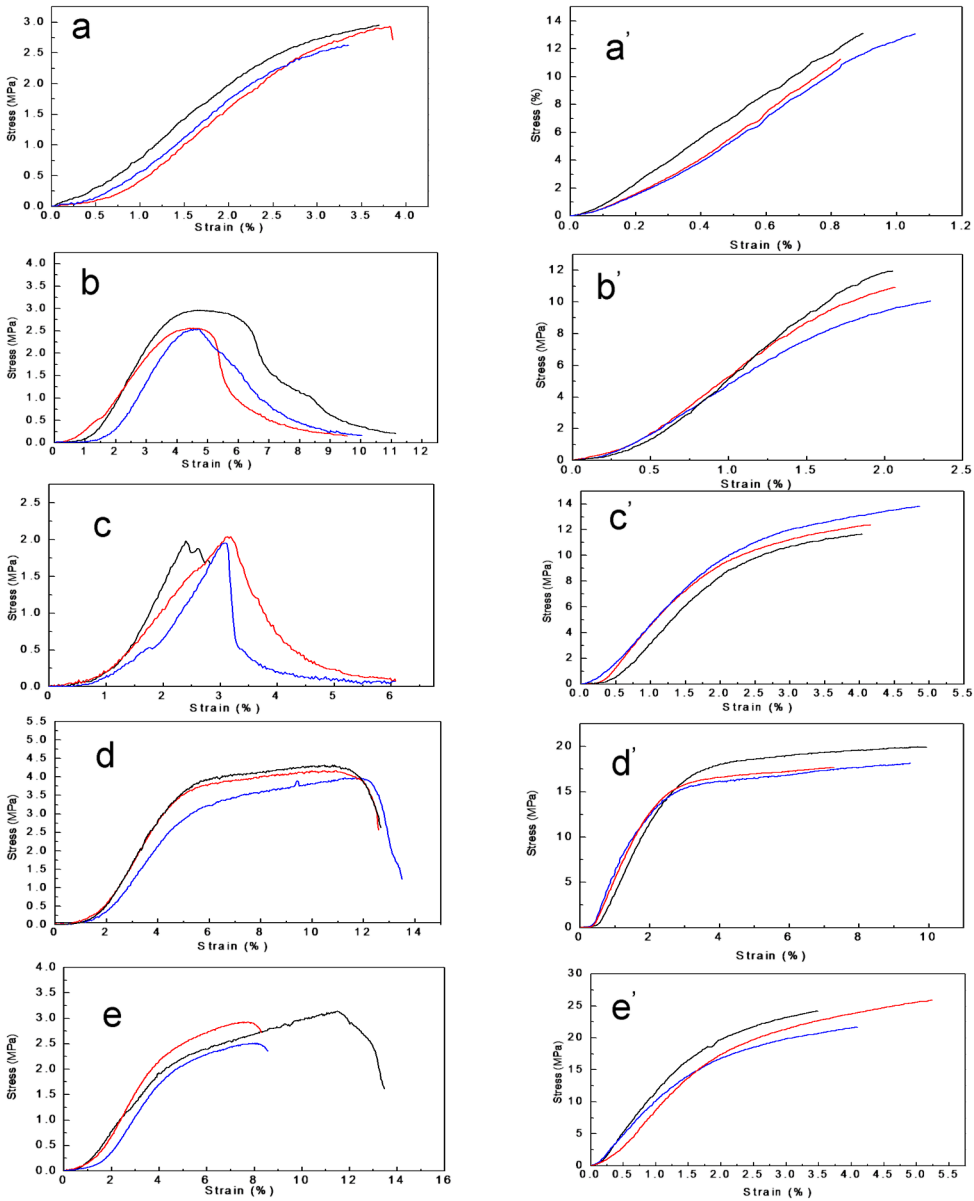

Figure 6. Stress–strain curves of SF/HBC nanofibrous scaffolds with different ratios before and after cross-linking: (a, a′) 100:0, (b, b′) 80:20, (c, c′) 50:50, (d, d′) 20:80 and (e, e′) 0:100. This figure is published in colour in the online edition of this journal, that can be accessed *via* http://www.brill.nl/jbs

crease in mean pore radius [30]. Suitable porous structure can be tailored through adjusting different ratios of SF/HBC.

Typical tensile stress–strain curves of SF/HBC blend nanofibrous scaffolds before and after cross-linking are shown in Fig. 6. The average elongation-at-break

Table 2.
Mechanical properties of SF/HBC nanofibrous scaffolds with various blend ratios

SF/HBC weight ratio			Average specimen thickness (mm)	Average elongation-at-break (%)	Average tensile strength (MPa)
100:0	Dry	Non-cross-linked	0.050 ± 0.005	3.85 ± 0.30	2.72 ± 0.60
		Cross-linked	0.057 ± 0.008	0.93 ± 0.11	12.48 ± 1.05
	Wet		–	–	–
80:20	Dry	Non-cross-linked	0.163 ± 0.021	2.89 ± 0.41	1.99 ± 0.04
		Cross-linked	0.059 ± 0.016	2.13 ± 0.13	11.00 ± 0.96
	Wet		0.078 ± 0.013	8.26 ± 0.78	0.67 ± 0.13
50:50	Dry	Non-cross-linked	0.169 ± 0.023	4.70 ± 0.10	2.68 ± 0.24
		Cross-linked	0.061 ± 0.011	4.33 ± 0.45	12.66 ± 1.12
	Wet		0.070 ± 0.013	18.32 ± 0.28	0.64 ± 0.17
20:80	Dry	Non-cross-linked	0.068 ± 0.014	11.04 ± 0.88	4.35 ± 0.45
		Cross-linked	0.047 ± 0.007	8.88 ± 1.42	18.65 ± 1.22
	Wet		0.089 ± 0.010	25.41 ± 1.28	1.52 ± 0.28
0:100	Dry	Non-cross-linked	0.060 ± 0.004	9.34 ± 3.04	2.66 ± 0.20
		Cross-linked	0.049 ± 0.005	4.26 ± 0.89	23.86 ± 1.99
	Wet		0.068 ± 0.017	19.35 ± 1.10	0.30 ± 0.19

Data are representative of six independent experiments and all are given as means ± SD.

and average tensile strength of each specimen in the dry state and wet state are summarized in Table 2. Pure SF nanofibrous scaffolds showed a typical brittle fracture; the average elongation-at-break was only 3.85 ± 0.30% and the average tensile strength was 2.72 ± 0.60 MPa. At SF/HBC blend ratios of 80:20 and 50:50, the stress of nanofibrous scaffolds gradually increased up to 1.99 MPa and 2.68 MPa and then began to decrease, respectively. In the experiment, we found that their nanofibrous scaffolds were so loose that some parts of the nanofibrous scaffolds were torn when scaffolds were stretched. This may be caused by the slippage among nanofibres rather than the break of fibres. Both the tensile strength and elongation-at-break were improved obviously when the weight ratio was 20:80. Thus, the mechanical properties were commendably improved in comparison with both pure SF and pure HBC. After cross-linking with genipin vapour for 24 h, SF/HBC nanofibrous scaffolds with different ratios exhibited a much higher tensile strength and lower elongation-at-break in comparison with non-cross-linked scaffolds. This was mainly ascribed to the inter/intramolecular covalent bonds and the physical entanglements among the nanofibres formed, whereby the sliding among chains and fibres decreased, which significantly improved the overall tensile strength. Among nanofibrous scaffolds of different ratios, nanofibrous scaffolds with a ratio of 20:80 had better mechanical properties after cross-linking. Mechanical tests of pure SF scaffolds in the wet state could not be carried out because the tenacity was too

poor to be measured. Compared with the dry nanofibrous scaffolds, all the average tensile strength obviously decreased, whereas all the average elongation-at-break increased to some extent after the nanofibrous scaffolds were soaked (Table 2). The plasticizing effect of water might be contributed to the tensile behaviour of soaked SF/HBC blend nanofibrous scaffolds.

3.5. Viablity of PIECs on Nanofibrous Scaffolds

The electrospun micro/nanofibers could provide a preferable matrix for cell adhesion and proliferation by the method of mimicking the natural ECM in the body. PIECs were seeded to evaluate cell adhesion and proliferation on the electrospun SF/HBC nanofibrous scaffolds. The viability of PIECs on days 1, 3, 5 and 7 after seeding on various nanofibrous scaffolds is shown in Fig. 7. It was revealed that all the nanofibrous scaffolds had good cell viability in comparison with coverslips. On day 3 and day 5, proliferation on pure SF, SF/HBC (80:20) and SF/HBC (50:50) nanofibreous scaffolds was increased significantly ($P \leqslant 0.01$ on day 3 and $P \leqslant 0.05$ on day 5) compared to coverslips. On day 7, proliferation on pure SF, SF/HBC (80:20), (50:50) and (20:80) nanofibrous scaffolds was also significantly higher ($P \leqslant 0.01$) than on coverslips. The results showed that pure SF and blened nanofibreous scaffolds could promote greater cell growth and proliferation. However, in comparison cell proliferation on pure HBC nanofibrous scaffolds had a lower increase speed. In general, scaffolds fabricated by pure SF and SF/HBC exerted positive effects on cell growth and proliferation compared to TCP.

Cell morphology and the interaction between cells and electrospun SF scaffolds were studied *in vitro* for 3 days, as shown in Fig. 8. After 3 days, PIECs attached and spread on the surface of pure SF, SF/HBC with different weight ratios nanofibrous scaffolds and formed a typical confluent endothelial monolayer. In contrast, PIECs

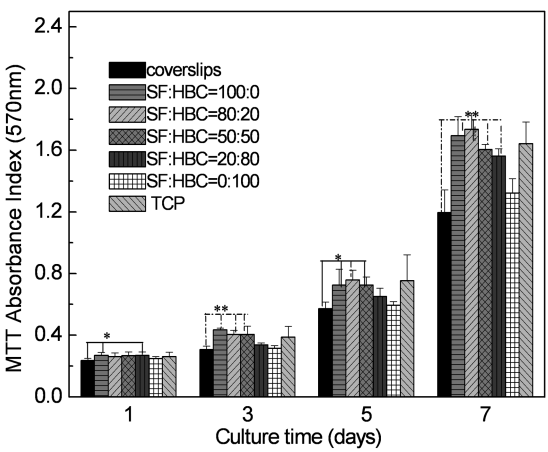

Figure 7. Proliferation of PIECs cultured on SF/HBC nanofibrous scaffolds, coverslips and TCP for 1, 3, 5 and 7 days. Data are expressed as mean ± SD ($n = 4$). Statistical difference between groups is indicated ($^{*}P < 0.05$; $^{**}P < 0.01$).

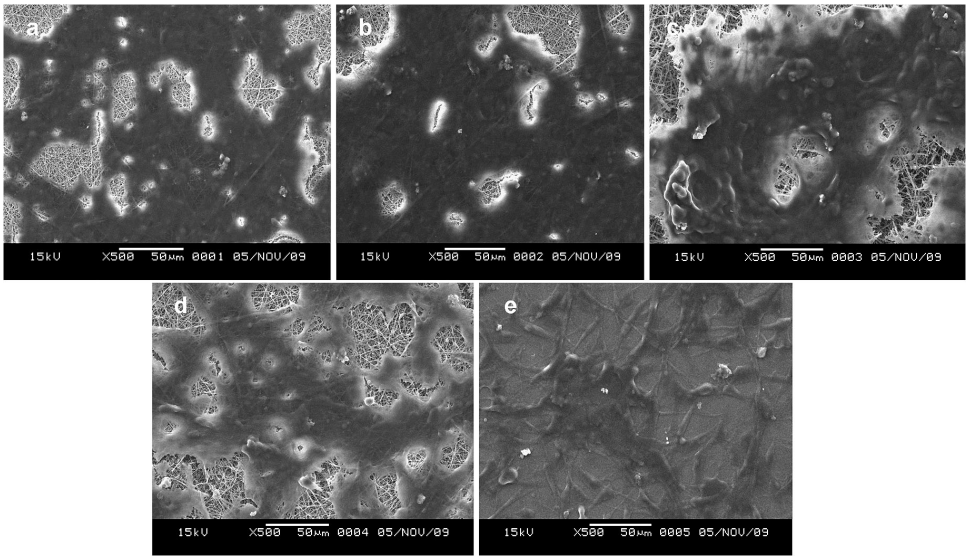

Figure 8. SEM micrographs of PIECs grown on nanofibrous scaffolds for 3 days: (a) 100:0, (b) 80:20, (c) 50:50, (d) 20:80 and (e) 0:100.

could not spread greatly on pure HBC nanofibrous scaffolds to form a confluent endothelial monolayer. This is because the swelling of HBC nanofibrous scaffolds in culture medium would lead to the loss of nanofibrous structure. The results illustrate that nanofibrous scaffolds were more favourable in the process of endothelialization than films. Therefore, SF/HBC nanofibrous scaffolds that biomimic the ECM might be beneficial to endothelial cells seeding or scaffold vascularization for tissue engineering.

4. Conclusions

Chitosan and *Bombyx mori* silk fibroin (SF) are the most abundant polysaccharide and protein in nature. In this study, SF/HBC nanofibrous scaffolds with different weight ratios were fabricated by electrospinning to biomimic the native ECM. SF/HBC nanofibrous scaffolds with different ratios possessed good hydrophilicity and both the tensile strength and elongation-at-break were improved when the weight ratio of SF to HBC reached 20:80. Cell behaviour on nanofibrous scaffolds showed that PIECs proliferated well on the nanofibre and formed typical confluent endothelial monolayer. These results strongly support that the SF/HBC nanofibrous scaffolds of similar components and the nanometer-scale architecture of ECM are conducive to tissue regeneration.

Acknowledgements

This research was supported by national high technology research and developed program (863 Program, 2008AA03Z305), Science and technology commission of

Shanghai municipality program (08520704600 and 0852 nm 03400), '111 Project' Biomedical textile materials science and technology (B07024), State Key Laboratory for Modification of Chemical Fibers and Polymer Materials Research Program (LZ0906) and the Shanghai–Unilever Research and Development Fund (08520750100).

References

1. C. Y. Xu, R. Inai, M. Kotaki and S. Ramakrishna, *Biomaterials* **25**, 877 (2004).
2. K. A. Gross and L. M. Rodríguez-Lorenzo, *Biomaterials* **25**, 4955 (2004).
3. I. Nishimura, R. L. Garrell, M. Hedrick, K. Iida, S. Osher and B. Wu, *Tissue Eng*. **9**, 77 (2003).
4. K. J. Shields, M. J. Beckman and G. L. Bowlin, *Tissue Eng*. **10**, 1510 (2004).
5. Z. W. Ma, M. Kotki, R. Inai and S. Ramakrishna, *Tissue Eng*. **11**, 101 (2005).
6. B. M. Min, G. Lee, S. H. Kim, Y. S. Nam, T. S. Lee and W. H. Park, *Biomaterials* **25**, 1289 (2004).
7. M. Wang, H. J. Jin, D. L. Kaplan and G. C. Rutledge, *Macromolecules* **37**, 6856 (2004).
8. M. Santin, A. Motta, G. Freddi and M. Cannas, *J. Biomed. Mater. Res*. **46**, 382 (1999).
9. R. L. Horan, K. Antle, A. L. Collette, Y. Z. Huang, J. Huang, J. E. Moreau, V. Volloch, D. L. Kaplan and G. H. Altman, *Biomaterials* **26**, 3385 (2005).
10. B. I. Thanou, M. Florea, H. E. Geldof, H. E. Junginger and G. Borchard, *Biomaterials* **23**, 153 (2002).
11. J. M. Dang and K. W. Leong, *Adv. Mater.* **19**, 2775 (2007).
12. B. Y. Chen, J. Y. Dang, T. L. Tan, N. Fang, W. N. Chen, K. W. Leong and V. Chan, *Biomaterials* **28**, 1503 (2007).
13. J. M. Dang, D. D. N. Sun, Y. Shin, A. N. Sieber, J. P. Kostuik and K. W. Leong, *Biomaterials* **27**, 406 (2006).
14. Z. D. She, C. R. Jin, Z. Huang, B. F. Zhang, Q. L. Feng and Y. X. Xu, *J. Mater. Sci. Mater. Med*. **19**, 3545 (2008).
15. M. C. Yang, S. S. Wang, N. K. Chou, N. H. Chi, Y. Y. Huang, Y. L. Chang, M. J. Shieh and Z. W. Chung, *Biomaterials* **30**, 3757 (2009).
16. W. J. Li, C. T. Laurencin, E. J. Caterson, R. S. Tuan and F. K. Ko, *J. Biomed. Mater. Res*. **60**, 613 (2002).
17. W. H. Park, L. Jeong, D. I. Yoo and S. Hudson, *Polymer* **45**, 7151 (2004).
18. Z. M. Huang, Y. Z. Zhang, S. Ramakrishna and C. T. Lim, *Polymer* **45**, 5361 (2004).
19. K. Ohkawa, D. Cha and H. Kim, *Macromol. Rapid Commun*. **25**, 1600 (2004).
20. X. H. Zong, K. Kim, D. F. Fang, S. F. Ran, B. S. Hsiao and B. Chu, *Polymer* **43**, 4403 (2002).
21. X. Chen, Z. Z. Shao, N. S. Marinkovic, L. M. Miller, P. Zhou and M. R. Chance, *Biophys. Chem*. **89**, 25 (2001).
22. P. Zhou, G. Y. Li, Z. Z. Shao, X. Y. Pan and T. Y. Yu, *J. Phys. Chem. B* **105**, 12469 (2001).
23. Q. X. Ruan and P. Zhou, *J. Mol. Struct*. **883**, 85 (2008).
24. M. F. Cervera, J. Heinamaki, M. Rasanen, S. L. Maunu, M. Karjalainen, O. M. Nieto Acosta, A. Iraizoz Colartea and J. Yliruusi, *Carbon Polym*. **58**, 401 (2004).
25. T. Asakura, M. Iwadate, M. Demura and M. P. Williamson, *Int. J. Biol. Macromol.* **24**, 167 (1999).
26. D. L. Bartolo, S. Morelli, A. Bader and E. Drioli, *J. Mater. Sci. Mater. Med.* **12**, 959 (2001).
27. M. Lampin, R. Warocquier-Clérout, L. M. Degrange and M. F. Sigot-Luizard, *J. Biomed. Mater. Res*. **36**, 99 (1997).
28. R. Murugan and S. Ramakrishna, *Tissue Eng*. **12**, 435 (2006).
29. S. J. Eichhorn and W. W. Sampson, *J. Roy. Soc. Interfaces* **2**, 309 (2005).
30. D. P. Li, M. W. Frey and Y. L. Joo, *J. Membr. Sci*. **286**, 104 (2006).